Mishina Yuji (Orcid ID: 0000-0002-6268-4204)

Podoplanin is dispensable for mineralized tissue formation and maintenance in the Swiss outbred mouse background.

Masako Toda Nakamura*[,1,2], Honghao Zhang*[,1], Dayong Guo*[,3], Hiroki Ueharu[1], Haichun Pan[1], Greg Scott[4], Marie Harris[3,5], Manas Ray[4], Jiang Q. Feng[3,6], Stephen E. Harris[3,5], Lynda F. Bonewald[3,7], and Yuji Mishina[1]

[1]Department of Biologic and Materials Sciences & Prosthodontics, School of Dentistry, University of Michigan, MI 48109, USA
[2]Section of Pediatric Dentistry, Department of Oral Growth and Development, Fukuoka Dental College, Fukuoka, Japan
[3]Department of Oral Biology, School of Dentistry, University of Missouri-Kansas City, MO 64108, USA
[4]Knock Out Core, National Institute of Environmental Health Sciences, National Institutes of Health, Research Triangle Park, NC 27709, USA
[5]UT Health San Antonio, Graduate School of Biomedical Sciences, San Antonio, TX 78229, USA
[6]Department of Biomedical Sciences, Texas A&M College of Dentistry, Dallas, TX 75246, USA
[7]Indiana Center for Musculoskeletal Health and Department of Anatomy, Cell Biology and Physiology, Indiana University, Indianapolis, IN 46202, USA

*, equal contribution

Running Title: The function of PDPN in mineralized tissue.

Key Words: Podoplanin, craniofacial development, osteocyte, tooth bud, skeletogenesis, exercise

Corresponding Author
Yuji Mishina, PhD
Professor
University of Michigan
School of Dentistry
Department of Biologic and Materials Sciences & Prosthodontics
1011 N. University Avenue
Ann Arbor, MI 48109-1078
Phone: 1-734-763-5579
Fax: 1-734-647-2110
E-mail: mishina@umich.edu

Abstract

Podoplanin, PDPN, is a mucin-type transmembrane glycoprotein widely expressed in many tissues, including lung, kidney, lymph nodes, and mineralized tissues. Its function is critical for lymphatic formation, differentiation of type I alveolar epithelial lung cells, and for bone response to biomechanical loading. It has previously been shown that *Pdpn* null mice die at birth due to respiratory failure emphasizing the importance of *Pdpn* in alveolar lung development. During the course of generation of *Pdpn* mutant mice, we found that most *Pdpn* null mice in the 129S6 and C57BL6/J mixed genetic background die at the perinatal stage, similar to previously published studies with *Pdpn* null mice, while all *Pdpn* null mice bred with Swiss outbred mice survived. Surviving mutant mice in the 129S6 and C57BL6/J mixed genetic background showed alterations in the osteocyte lacunocanalicular network, especially reduced osteocyte canaliculi in the tibial cortex with increased tibial trabecular bone. However, adult *Pdpn* null mice in the Swiss outbred background showed no overt differences in their osteocyte lacunocnalicular network, bone density, and no overt differences when challenged with exercise. Together, these data suggest that genetic variations present in the Swiss outbred mice compensate for the loss of function of PDPN in lung, kidney, and bone.

1 INTRODUCTION

Podoplanin (PDPN), also known as E11, gp38, RTI40, or T1 alpha, is a mucin-type transmembrane glycoprotein widely expressed in many tissues such as lung, kidney, lymph nodes, and mineralized tissues (Schulze et al., 1999; Astarita et al., 2012). PDPN is extensively O-glycosylated with a high content of sialic acid (Gonzalez and Dobbs 1998). PDPN interacts with a variety of intracellular and transmembrane proteins to mediate effects on cell migration and adhesion (Prideaux et al., 2012). Binding of PDPN to CD44 or ezrin/radixin/moesin (ERM) proteins results in increased cell migration and rearrangement of the actin cytoskeleton to generate actin-rich protrusions of the membrane (Martin-Villar et al., 2010; Prideaux et al., 2012). PDPN is thought to be involved in the development and homeostatic maintenance of several kinds of cells and tumorigenesis (Renart et al., 2015; Suzuki-Inoue et al., 2017; Retzbach et al., 2018).

Pdpn is expressed in osteocytes and osteoblasts (Zhang et al., 2006), choroid plexus (Zhang et al., 2006), perineurium (Noda et al., 2010), tooth germ epithelial cells (Imaizumi et al., 2010), salivary gland myoepithelium (Amano et al., 2011), thymus type I epithelial cells, prostate myofibroblasts, follicular dendritic cells, and immature cells such as fetal germ cells and developing Sertoli cells. *Pdpn* is expressed by budding *Prox1*-positive lymphatic progenitor cells around embryonic day 11, E11.0 (Schacht et al., 2003). *Pdpn* null mice die at birth because of respiratory failure associated with reduced numbers of differentiated type I alveolar epithelial cells in the lung (Ramirez et al., 2003). The expression of *Pdpn* is also restricted to *Prox1*-positive lymphatic endothelial cells of the lymph sac (Schacht et al., 2003; Groger et al., 2004). Lack of *Pdpn* leads to alterations in the final patterning of the lymphatic vasculature as well as in lymph transport. *Pdpn* null mice also have defects in lymphatic formation with diminished lymphatic transport and congenital lymphedema (Schacht et al., 2003).

Pdpn is expressed in craniofacial tissues, for example, tongue, bone, muscle, and tooth (Zhang et al., 2006; Sawa et al., 2008; Imaizumi et al., 2010; Noda et al., 2010). Within bones, PDPN is only found in the dendritic processes of osteocytes, and not found in osteoblasts *in vivo* (Zhang et al., 2006; Bonewald 2011). These studies also show that PDPN is localized within osteocyte membranes and at punctate vesicles at the interface between osteocytes and uncalcified osteoid cells (Schulze et al., 1999; Zhang et al., 2006). Expression of *Pdpn* in the dendritic processes of osteocytes is increased in response to mechanical strain *in vitro* (Zhang et al., 2006). PDPN is also found in enamel epithelia (Sawa et al., 2008), odontoblasts (Imaizumi et al., 2010), and cementocytes (Zhao et al., 2016). PDPN expression and location suggest roles in skeletogenesis and craniofacial development. Indeed, conditional deletion of *Pdpn* in bone cells using *Osteocalcin*-Cre results in a significant reduction in dendrite volume and length in association with improved biomechanical properties such as resistance to higher fracturing load (Staines et al., 2017). These transgenic mice also showed resistance against load-induced osteoarthritis and ovariectomy induced osteoclast activation (Staines et al., 2019; Staines et al., 2020), demonstrating important roles of PDPN in bone strength and function.

During the course of generation and analyses of *Pdpn* mutant mice where loxP insertion resulted in hypomorphs (Prideaux et al., 2015), we discovered that neonatal lethality varies depending on genetic background. Despite a high mortality rate for homozygous mutant mice for the floxed

allele of *Pdpn* in a mixed background of 129S6 and C57BL6/J (129/B6), all survived when bred with Swiss outbred mice twice. In this report, we examined possible skeletal phenotypes in surviving mice in the 129/B6 mixed background and in the Swiss outbred background to identify potential functions of PDPN in skeletogenesis.

2 MATERIALS AND METHODS

2.1 Mouse Breeding and genotyping

Generation of the podoplanin (*Pdpn*) mutant allele was reported previously (Prideaux et al., 2015). In brief, one loxP was inserted into the 5'-UTR of the exon 1 and the other loxP was inserted into the 1st intron (Supplementary Fig. 1). Details of the initial screening strategy of targeted embryonic stem cells (AB2.2 and UG347 lines) and subsequent genotyping strategy using PCR are summarized in Supplementary Figure 1. After removal of the neo cassette by crossing with Flipper mice (Farley et al., 2000), we set up breeding between $Pdpn^{fl/+}$ mice and $Pdpn^{fl/+};Ocn$-Cre mice to disrupt *Pdpn* in the osteoblast lineage (Zhao et al., 2002). Later, heterozygous mice ($Pdpn^{fl/+}$) were bred with *Sox2*-Cre transgenic mice (Hayashi et al., 2003) to remove the floxed region to inactivate gene function (Cre-recombined allele, designated '-' hereafter). Homozygous mice for the Cre-recombined allele ($Pdpn^{-/-}$) were generated by intercrossing of the Cre-recombined heterozygous mice. Noon of the date when the vaginal plug observed was designated as E0.5. Genotypes were determined by PCR analyses; primers A and B were used to amplify fragments from wildtype (187 bp) and the *Pdpn* floxed alleles (292 bp for fx). Primers C and B were used to detect presence of the neomycin selection cassette (400 bp). Primers D and B were used to detect Cre-dependent deletion of the floxed region (348 bp for '-') (Supplementary Figure 1). Sequences for genotyping primers are: A (5'-CCCTAACAACCCCCTCCGC-3'), B (5'-CCTCTTCAGGTCTATCCCCAGCC-3'), C (5'-ACCGACACTCAGCACCATTTCC-3'), D (5'-ATAAATGCCGACTGTGCCGAGAGG-3'). The mutations are maintained in a mixture of 129S6 and C57BL6/J. In some cases, the mutant mice were backcrossed twice or more with Swiss Webster outbred mouse stock (Taconic). All mouse experiments were performed in accordance with institutional guidelines covering the humane care and use of animals in research. The animal protocols were approved by the Institutional Animal Care and Use Committees at the National Institute of Environmental Health Sciences, the University of Missouri at Kansas City, and the University of Michigan.

2.2 Quantification of *Pdpn* Gene expression

Approximately 100 mg of tissue was collected from lung, intestines, kidney and bone of 3-month-old male mice followed by total RNA extraction using TRIzol Reagent, catalog number 15596-026 (Invitrogen, Carlsbad, CA, USA), according to the manufacturer's instructions. Reverse transcription was performed with 100 ng of total RNA using the High Capacity cDNA Reverse Transcription Kit, catalog number 4368814 (Applied Biosystems, Foster City, CA, USA). Real time PCR was conducted with TaqMan Gene Expression Assays designed for mouse E11/gp38, catalog number 4331182 (Applied Biosystems). TaqMan Rodent GAPDH Control Reagents, catalog number 4308313 (Applied Biosystems) was used as an internal control. Quantitative PCR was conducted on an ABI Prism 7000 Sequence Detection System (Applied Biosystems) following the manufacturer's instructions. The final expression level of *Pdpn* mRNA was normalized as a ratio to the GAPDH mRNA level from the same sample.

2.3 Histology, skeletal staining, and immunocytochemistry

Embryos or adult tissue was fixed in 4% paraformaldehyde (PFA), dehydrated, and embedded in paraffin. Seven μm sections were cut and stained with hematoxylin and eosin (H&E), Picrosirius red or Von Kossa according to standard procedures. For immunodetections, embryos or adult tissues were fixed in 4% PFA at 4°C overnight followed by incubation in 20% sucrose/PBS at

4°C for overnight, embedded in O.C.T. compound (Sakura Finetek, Tokyo, Japan), and serially sectioned in 10 µm. The samples were incubated with hamster anti-Podoplanin (1:100 dilution, sc-53533, Santa Cruz Biotechnology, Santa Cruz, CA, USA), goat anti-Amelogenin (1:100 dilution, sc-365284, Santa Cruz Biotechnology, Santa Cruz, CA, USA), at 4°C overnight. Alexa Fluor 488 goat Anti-Syrian Hamster IgG or Alexa Fluor 488 goat anti-mouse IgG1 (1:100 dilution, A21121, Invitrogen) were used as secondary antibodies. For kidney and lung, serially sectioned paraffin sections were incubated with an E11 antibody against Podoplanin (1:100 dilution, a kind gift from Dr. Andrew Farr) and subsequently incubated with a peroxidase-conjugated goat anti-Syrian hamster IgG (sc-2905, Santa Cruz Biochemistry) then color developed using a DAB substrate kit (Vector Laboratories). For bones, Cy3 goat anti-hamster IgG (Jackson ImmunoResearch Laboratories, 107-165-142) was used for detection. For liver analyses, the following antibodies were used: CD90, which specifically marks Hepatic progenitor cells: AB3105 (Abcam), Rat antibody, Anti-Rat-Alexa fluor 488; Albumin: MAB 1455 (R & D system), Mouse antibody, Anti-Mouse-Alexa fluor 595, and E11, Sc53533 (Santa Cruz), Hamster antibody, Anti-Hamster-Alexa fluor 488. Sections were mounted with ProLong Gold antifade reagent with DAPI (P36935, Invitrogen). Intensity of fluorescent signal was quantified using ImageJ 1.53J.

2.4 Scanning electron microscopy (SEM) and Osteoimaging
Samples were first fixed in 70% ethanol for 3 days and then transferred to 100% ethanol to dehydrate under vacuum overnight. Next, they were put into 10 ml infiltration solution (methylmethacrylate 8.5 ml, dibutylphthalate 1.4 ml, polyethylene glycol 400 100 µl and benzoyl peroxide 70 mg) and shaken at room temperature for 4 days. Ten ml embedding solution (methylmethacrylate 8.5 ml, dibutylphthalate 1.4 ml, polyethylene glycol 400 100 µl, and benzoyl peroxide 400 mg) was prepared in a glass vial on ice. N, N-dimethyl-p-toluidine, 33 µl added as an accelerator into the vial, and the samples were then placed in the vial followed by purging with nitrogen. The vials were tightly capped and kept at 4ºC until polymerization was complete. Embedded samples were trimmed and polished to expose the bone surface, then cleaned with a sonicating machine. Phosphoric acid (37%) was used to etch the surface for 10 seconds, followed by bleaching with 5% sodium hypochlorite for 5 minutes. After washing and air drying, the surface was coated with palladium and gold, and examined under a Philips SEM 515 scanning electron microscope in the secondary electron mode.

The SEM images of acid etched bone surfaces revealed the configuration of the lacuno-canalicular network in bone. Four images were taken from each sample. The distances between an osteocyte and its three nearest neighbors were measured, averaged and compared between the control and mutant bones. The density of canaliculi was determined at a site which is 10 microns beneath the endosteal surface of cortical bone at the mid-shaft of both the ulna and tibia, and 1-2 mm below the proximal growth plate in the trabecular bone of the tibia.

2.5 microCT analyses
Tibias from 3-month-old male mice were analyzed using a µCT 40 x-ray machine (Scanco Medical, Southwestern, PA, USA) with a resolution of 15 µm and a threshold of 300 Hounsfield units. Cortical total volume, cortical bone volume, cortical thickness, cortical apparent density of bone and marrow, cortical material density of bone were measured at the mid-shaft (-1 to +1 mm). Trabecular bone volume / total volume, trabecular number, trabecular thickness, trabecular

apparent density of bone and marrow, and trabecular material density of bone were measured at 1 to 2 mm below the growth plate.

2.6 Exercise on treadmill
Four-month-old males and females (n=4 for each gender, n=4 for $Pdpn^{+/+}$ or $Pdpn^{-/-}$) were exercised for three weeks. Each exercise session lasted 30 minutes and the average speed was 12 meter/min at a 5° incline (Iura et al., 2015). One day after the end of the exercise regime, at 5 months of age, all the mice were euthanized, and femora were removed.

2.7 Statistical Analysis
One-way ANOVA with Bonferroni's post test was used to conduct statistical comparisons among multiple groups. If there were only two groups, unpaired two-tailed t-test was used. The threshold for statistical significance was set to be $p<0.05$. All computations were performed with GraphPad Prism version 3.0 (GraphPad Software, San Diego, CA, USA).

3 RESULTS

3.1 The floxed *Pdpn* allele is highly hypomorphic resulting in an abnormal osteocyte morphology

Floxed mice were generated in a 129S6/C57BL6 background (129/B6) through homologous recombination in embryonic stem cells (Supplementary Figure 1). Homozygous mice for the floxed allele showed perinatal lethality due to lung malfunction (Table 1). While homozygous mice for the floxed allele ($Pdpn^{fl/fl}$) were present in the Mendelian ratio at E18.5, the expected number of homozygous mice was drastically reduced at the 3 weeks of age. Removal of the neo-cassette from the locus did not improve the lethality on the 129/B6 background (Table 1). We speculate this is probably due to the insertion of the 5' loxP site into a 5'UTR region of exon 1 compromising expression of *Pdpn* (Supplementary Fig. 1). This concept was supported by the observations that levels of *Pdpn* mRNA from 1 month old tibia, kidney, and lung of the homozygous mice for the floxed allele are below detection (Fig 1A-C). mRNA levels in the heterozygous tissues were significantly reduced, but PDPN proteins was detected by immunohistochemistry at comparable intensity to wild type, while no signal was observed in the homozygous tissues (Fig 1D).

We took an advantage of the tissue-specific gene disruption strategy to disrupt endogenous *Pdpn* using an *Osteocalcin-Cre* (*Ocn-Cre*), which is expressed in late osteoblasts to early osteocytes (Zhao et al., 2002) to insure ablation of *Pdpn* in the osteoblast lineage, in order to investigate potential bone phenotypes of the surviving mutant mice in 129/B6 background. While heterozygous mice for the floxed allele of *Pdpn* ($Pdpn^{fl/+};Ocn-Cre$) showed detectable immunosignal of PDPN especially in areas of newly embedded osteocytes, no signal was observed level in bones from $Pdpn^{fl/fl};Ocn-Cre$ mice. (Fig 1E).

Among the limited number of surviving mice at 3-months of age ($Pdpn^{fl/fl};Ocn-Cre$), there were two classes of mutant mice: normal sized with normal appearance (n=4) and smaller size with ascites (n=2) (Fig 2A). The normal appearing mutant mice displayed alterations in the lacunocanalicular network in the cortex of their tibia (Fig 2B, C). The number of canaliculi was

reduced to half, while no significant change in the average distance between the 3 nearest neighboring osteocytes was observed (Fig 2D, E). The microCT analyses revealed a significantly higher volume in the trabecular compartment of the tibia (Fig 2F). This is mainly due to an increase in trabecular number resulting in an increase of apparent density in the mutant bones. Cortical compartments did not show significant differences between two genotypes (Fig 2G).

3.2 *Pdpn* does not play a role in embryonic mineralized tissue development

After removal of the floxed segment of *Pdpn* to generate a Cre-recombined allele (= functionally null, designated '-' hereafter) (Fig 3A), we set up intercrosses between heterozygous mutant mice for the Cre-recombined allele. As expected, *Pdpn*$^{-/-}$ mice died soon after birth showing impaired formation of alveolar airspace (Fig. 3B) resembling the previously reported phenotype found in homozygous *Pdpn* mutant mice deficient in exon 1 (Ramirez et al., 2003). For possible skeletal phenotypes, we investigated calvaria, tibial growth plate and metaphysis. Histologic observation of H&E stained sections did not show overt changes in these bones (Fig. 3C). Osteoblasts and osteocytes were present in *Pdpn*$^{-/-}$ mice similar to controls. Since *Pdpn* is highly expressed in early osteocytes (Zhang et al., 2006), we examined mineral deposition and collagen maturation to determine potential functional changes of osteoblasts and osteocytes. By Picrosirius Red staining, there were no significant differences in collagen fibers as *Pdpn*$^{-/-}$ mice showed mature collagen type1 fibers (Fig. 3C). Also, there were no significant differences in Von Kossa stain (Fig. 3C) between *Pdpn*$^{-/-}$ mice and wildtype mice with regards to their calcified bone matrix. This result suggests that PDPN does not play critical role in skeletogenesis during embryogenesis.

Pdpn is expressed in enamel epithelial cells (Imaizumi et al., 2010). To characterize the tooth phenotype in these mice, we conducted histologic and immunostaining analyses at E18.5 (Fig. 4). *Pdpn*$^{-/-}$ mice did not show any tooth morphological changes; no significant differences in inner enamel epithelium, pre-dentin, or the odontoblasts layers (Fig. 4, left). Polarization of ameloblasts was also observed in *Pdpn*$^{-/-}$ mice. PDPN locates in the inner enamel epithelia, pre-dentin, and odontoblast layers of wild type mice. This result suggests that PDPN is produced from odontoblasts to inner enamel epithelia (Fig. 4, right and (Imaizumi et al., 2010)). No immunosignal for PDPN further shows that the homozygous mice we generated here are null for *Pdpn* (Fig. 4, right). To better understand the effect of loss of *Pdpn* in tooth bud development, we examined distribution of amelogenin, a marker for ameloblasts. However, no significant differences were observed in the incisor and molar between controls and mutants (Fig. 4).

A limited number of homozygous mutant mice for the Cre-recombined allele (*Pdpn*$^{-/-}$) in 126S6/C57BL6 background survived for up to several months (Table 2). However, similar to the *Pdpn*$^{fl/fl}$;*Ocn*-Cre mice in the 126S6/C57BL6 background, approximately half of them showed smaller body size by 1 month after birth, with ascites. To address potential reasons for this pathologic condition, we examined the liver from the smaller *Pdpn*$^{-/-}$ mice and compared to littermate controls (*Pdpn*$^{+/+}$) (Fig 5). Loss of PDPN signaling in *Pdpn*$^{-/-}$ liver further confirmed that the mice are null for *Pdpn*. Reduced signal intensity for albumin suggests that a reduction in albumin in the serum may be responsible for the ascites. An increase of CD90 signal, a marker for developmental hepatic cells, in the mutant livers further supports the hypothesis that PDPN is important for normal differentiation of hepatocytes.

3.3 Loss of *Pdpn* is compensated for in the Swiss outbred mouse background

Phenotypes from the same genetic manipulation can differ dramatically depending on mouse strain and genetic background (Mahtab et al., 2008; Mahtab et al., 2009). As mentioned earlier, we found that most of the homozygous mice for the floxed *Pdpn* allele (*Pdpn$^{fl/fl}$*) die at the perinatal stage likely due to lung malfunction (Table 1). When the mice were backcrossed to the Swiss outbred stock, the ratio of homozygous mice for the floxed allele were significantly higher at 3 weeks of age compared to the 129/B6 background (Table 1). As expected, these mice did not show the presence of PDPN in kidney, lung, or bones (Figure 6). The normal survival rate suggested compensation by another gene(s). This interpretation is further supported by the observation that homozygous mice for Cre-recombined allele (*Pdpn$^{-/-}$*) can survive to the age of 3 weeks with expected Mendelian ratios after twice of backcrossing with Swiss outbred mice (Table 2).

Since *Pdpn* is highly expressed in early osteocytes, we looked at osteocyte lacunar morphology in the tibia of 6-month-old mice in the Swiss outbred background (backcrossed twice or more, 75% or more was Swiss background). X-ray images from tibia, calvaria and lumbar vertebrae did not show any significant differences between control (*Pdpn$^{+/-}$*) and homozygous mutant mice (*Pdpn$^{-/-}$*) (Fig 7, A-C). Acid-etching did not reveal any overt differences in shape and number of osteocyte lacunae or canaliculi (Fig 7, D). After exercise of 4-month-old animals of the Swiss outbred background, no overt differences were noted between exercised control and the exercised mutant groups (*Pdpn$^{-/-}$*, 75% or more was Swiss background) (Fig 7, E).

4 DISCUSSION

Here we show that podoplanin (PDPN) can be dispensable or indispensable depending on the mouse genetic background. Our newly developed 129/B6 murine model carrying floxed alleles for podoplanin (*Pdpn$^{fl/fl}$*) showed significant perinatal lethality and those that survived showed severe hypomorphism. The surviving homozygous mutant mice in 129/B6 mixed background showed reduced numbers of canaliculi in osteocytes and increased trabecular bone volume. Homozygous mice for the Cre-recombined allele (*Pdpn$^{-/-}$*) die perinatally due to insufficient lung development as previously reported, but no overt changes were observed in the skeletal system including long bones and teeth. Hepatic malfunctions were found in surviving *Pdpn* floxed or null allele in the 129/B6 mixed background resulting in small size and ascites production. Surprisingly, this perinatal lethality does not occur with global deletion of *Pdpn* in the Swiss outbred background. Homozygous null mice (*Pdpn$^{-/-}$*) in the Swiss background did not show any overt bone phenotype or changes in osteocyte lacunocanalicular network nor an atypical response to exercise. These data suggest that unknown changes in gene expression may compensate for the loss of *Pdpn* in the Swiss background and that they may make PDPN be completely dispensable for physiologic skeletal formation and responses to the mechanoenvironment.

There are several reports using conditional mouse models for *Pdpn*. In a conditional mouse line floxing exon 3 of *Pdpn* crossed with an *Osteocalcin*-Cre mouse line, dendrite volume and length

were significantly reduced in 6-week-old mutant mice (Staines et al., 2017). This is in contrast to our data showing no overt changes in the length of canaliculi, suggesting that if loss of PDPN was compensated for during development, it would be no longer be required for bone homeostasis. It is reported that PDPN levels in osteocytes are increased in osteoarthritic subchondral bones from humans, canines, and mice (Staines et al., 2019). Conditional mutant mice for *Pdpn* showed resistance against load-induced osteoarthritis, suggesting that PDPN is involved in the pathogenesis of osteoarthritis (Staines et al., 2019). Mice with bone cell-specific disruption of *Pdpn* showed resistance to ovariectomy-induced bone loss (Staines et al., 2020). Interestingly, the increase in osteoclast activity due to ovariectomy was suppressed in the mutant mice despite alterations in the RANKL/OPG ratio, suggesting that PDPN plays a role in osteoblasts/osteocytes to support osteoclastogenesis through a mechanism independent of the RANKL/OPG axis (Staines et al., 2020). These data suggest that PDPN functions in bone cells to positively regulate osteoclast function, which could be one of the reasons of the increased trabecular bone mass in our *Pdpn* mutant mice in the mixed background. In contrast to our studies and the studies by Staines and colleagues, there is no overt tooth phenotype observed in 2-week-old *Pdpn* conditional mice using the neural crest-specific *Wnt1*-Cre line (Takara et al., 2017).

Initially, we aimed to develop a conditional mutant allele for *Pdpn* by floxing exon 1. We soon realized that homozygous mice for the floxed-neo allele resulted in perinatal lethality. Removal of the neomycin cassette from the targeted allele did not improve the lethality. Taking these data together, these results suggest that insertion of a loxP site in the 5'-UTR of exon 1 may result in lower expression of *Pdpn* expression or reduced stability of *Pdpn* mRNA. We found significant improvement in neonatal lethality after twice back-crossing to the Swiss outbred background, when theoretically 75% of the genome is replaced by the Swiss background. This is far less than the 5-10 back-crosses needed to produce a congenic strain. The homozygous mice in the Swiss background, which escape from lethality, still do not produce PDPN protein suggesting that these mutant mice are rescued, not because changes in *Pdpn* mRNA, but because other genes compensate for a lack of PDPN in the mutants. We are presently screening differentially expressed genes that could explain the compensation for lethality and the bone phenotype found in surviving *Pdpn* mutant mice. Candidate genes may include MT1-MMP, which is required for osteocyte processes (Holmbeck et al., 2005), and destrin, which is involved in cytoskeletal rearrangement (Guo et al., 2010).

Taken together, the conditional gene knockout approach reveals important functions of PDPN in skeletal homeostasis, but if early lethality is rescued in a different genetic background (Swiss outbred stock in this case), the rescued mice do not show any overt skeletal phenotypes even after application of mechanical loading. We hypothesize that some genes are up-regulated (or down-regulated) in the rescued mutant mice for *Pdpn* to compensate for the loss of PDPN, especially during type 1 cell differentiation in the lung, and that the rescued mice develop a skeletal system that no longer requires PDPN for its homeostasis. Of note, there are no known structurally related genes to PDPN. Identifying differentially expressed genes in the rescued mutant mice would be an important future direction to deepen our understanding of skeletal homeostasis.

Acknowledgement

Author Contribution
Study design: MTN, HZ, DG, JQF, LFB and YM. Materials to generate: DG, GS, MH, MR, SEH and YM. Study conduct: Data collection: Data analysis: MTN, HZ, DG, HU, HP, and YM. Data interpretation: MTN, HZ, DG, SEH, JQF, LFB and YM. Writing manuscript: MTN, HZ, DU, LFB and YM. Approving final version of manuscript: all authors. HZ and YM take responsibility for the integrity of the data analysis.

References

Amano I, Imaizumi Y, Kaji C, Kojima H, Sawa Y. 2011. Expression of podoplanin and classical cadherins in salivary gland epithelial cells of klotho-deficient mice. Acta Histochem Cytochem 44: 267-276.

Astarita JL, Acton SE, Turley SJ. 2012. Podoplanin: emerging functions in development, the immune system, and cancer. Front Immunol 3: 283.

Bonewald LF. 2011. The amazing osteocyte. J Bone Miner Res 26: 229-238.

Farley FW, Soriano P, Steffen LS, Dymecki SM. 2000. Widespread recombinase expression using FLPeR (flipper) mice. Genesis 28: 106-110.

Gonzalez RF, Dobbs LG. 1998. Purification and analysis of RTI40, a type I alveolar epithelial cell apical membrane protein. Biochim Biophys Acta 1429: 208-216.

Groger M, Loewe R, Holnthoner W, Embacher R, Pillinger M, Herron GS, Wolff K, Petzelbauer P. 2004. IL-3 induces expression of lymphatic markers Prox-1 and podoplanin in human endothelial cells. J Immunol 173: 7161-7169.

Guo D, Keightley A, Guthrie J, Veno PA, Harris SE, Bonewald LF. 2010. Identification of osteocyte-selective proteins. Proteomics 10: 3688-3698.

Hayashi S, Tenzen T, McMahon AP. 2003. Maternal inheritance of Cre activity in a Sox2Cre deleter strain. Genesis 37: 51-53.

Holmbeck K, Bianco P, Pidoux I, Inoue S, Billinghurst RC, Wu W, Chrysovergis K, Yamada S, Birkedal-Hansen H, Poole AR. 2005. The metalloproteinase MT1-MMP is required for normal development and maintenance of osteocyte processes in bone. J Cell Sci 118: 147-156.

Imaizumi Y, Amano I, Tsuruga E, Kojima H, Sawa Y. 2010. Immunohistochemical examination for the distribution of podoplanin-expressing cells in developing mouse molar tooth germs. Acta Histochem Cytochem 43: 115-121.

Iura A, McNerny EG, Zhang Y, Kamiya N, Tantillo M, Lynch M, Kohn DH, Mishina Y. 2015. Mechanical Loading Synergistically Increases Trabecular Bone Volume and Improves Mechanical Properties in the Mouse when BMP Signaling Is Specifically Ablated in Osteoblasts. PLoS One 10: e0141345.

Mahtab EA, Vicente-Steijn R, Hahurij ND, Jongbloed MR, Wisse LJ, DeRuiter MC, Uhrin P, Zaujec J, Binder BR, Schalij MJ, Poelmann RE, Gittenberger-de Groot AC. 2009. Podoplanin deficient mice show a RhoA-related hypoplasia of the sinus venosus myocardium including the sinoatrial node. Dev Dyn 238: 183-193.

Mahtab EA, Wijffels MC, Van Den Akker NM, Hahurij ND, Lie-Venema H, Wisse LJ, Deruiter MC, Uhrin P, Zaujec J, Binder BR, Schalij MJ, Poelmann RE, Gittenberger-De Groot AC. 2008. Cardiac malformations and myocardial abnormalities in podoplanin knockout mouse embryos: Correlation with abnormal epicardial development. Dev Dyn 237: 847-857.

Martin-Villar E, Fernandez-Munoz B, Parsons M, Yurrita MM, Megias D, Perez-Gomez E, Jones GE, Quintanilla M. 2010. Podoplanin associates with CD44 to promote directional cell migration. Mol Biol Cell 21: 4387-4399.

Noda Y, Amano I, Hata M, Kojima H, Sawa Y. 2010. Immunohistochemical examination on the distribution of cells expressed lymphatic endothelial marker podoplanin and LYVE-1 in the mouse tongue tissue. Acta Histochem Cytochem 43: 61-68.

Prideaux M, Dallas SL, Zhao N, Johnsrud ED, Veno PA, Guo D, Mishina Y, Harris SE, Bonewald LF. 2015. Parathyroid Hormone Induces Bone Cell Motility and Loss of Mature Osteocyte Phenotype through L-Calcium Channel Dependent and Independent Mechanisms. PLoS One 10: e0125731.

Prideaux M, Loveridge N, Pitsillides AA, Farquharson C. 2012. Extracellular matrix mineralization promotes E11/gp38 glycoprotein expression and drives osteocytic differentiation. PLoS One 7: e36786.

Ramirez MI, Millien G, Hinds A, Cao Y, Seldin DC, Williams MC. 2003. T1alpha, a lung type I cell differentiation gene, is required for normal lung cell proliferation and alveolus formation at birth. Dev Biol 256: 61-72.

Renart J, Carrasco-Ramirez P, Fernandez-Munoz B, Martin-Villar E, Montero L, Yurrita MM, Quintanilla M. 2015. New insights into the role of podoplanin in epithelial-mesenchymal transition. Int Rev Cell Mol Biol 317: 185-239.

Retzbach EP, Sheehan SA, Nevel EM, Batra A, Phi T, Nguyen ATP, Kato Y, Baredes S, Fatahzadeh M, Shienbaum AJ, Goldberg GS. 2018. Podoplanin emerges as a functionally relevant oral cancer biomarker and therapeutic target. Oral Oncol 78: 126-136.

Sawa Y, Iwasawa K, Ishikawa H. 2008. Expression of podoplanin in the mouse tooth germ and apical bud cells. Acta Histochem Cytochem 41: 121-126.

Schacht V, Ramirez MI, Hong YK, Hirakawa S, Feng D, Harvey N, Williams M, Dvorak AM, Dvorak HF, Oliver G, Detmar M. 2003. T1alpha/podoplanin deficiency disrupts normal lymphatic vasculature formation and causes lymphedema. EMBO J 22: 3546-3556.

Schulze E, Witt M, Kasper M, Lowik CW, Funk RH. 1999. Immunohistochemical investigations on the differentiation marker protein E11 in rat calvaria, calvaria cell culture and the osteoblastic cell line ROS 17/2.8. Histochem Cell Biol 111: 61-69.

Staines KA, Hopkinson M, Dillon S, Stephen LA, Fleming R, Sophocleous A, Buttle DJ, Pitsillides AA, Farquharson C. 2020. Conditional deletion of E11/Podoplanin in bone protects against ovariectomy-induced increases in osteoclast formation and activity. Biosci Rep 40.

Staines KA, Ikpegbu E, Tornqvist AE, Dillon S, Javaheri B, Amin AK, Clements DN, Buttle DJ, Pitsillides AA, Farquharson C. 2019. Conditional deletion of E11/podoplanin in bone protects against load-induced osteoarthritis. BMC Musculoskelet Disord 20: 344.

Staines KA, Javaheri B, Hohenstein P, Fleming R, Ikpegbu E, Unger E, Hopkinson M, Buttle DJ, Pitsillides AA, Farquharson C. 2017. Hypomorphic conditional deletion of E11/Podoplanin reveals a role in osteocyte dendrite elongation. J Cell Physiol 232: 3006-3019.

Suzuki-Inoue K, Osada M, Ozaki Y. 2017. Physiologic and pathophysiologic roles of interaction between C-type lectin-like receptor 2 and podoplanin: partners from in utero to adulthood. J Thromb Haemost 15: 219-229.

Takara K, Maruo N, Oka K, Kaji C, Hatakeyama Y, Sawa N, Kato Y, Yamashita J, Kojima H, Sawa Y. 2017. Morphological study of tooth development in podoplanin-deficient mice. PLoS One 12: e0171912.

Zhang K, Barragan-Adjemian C, Ye L, Kotha S, Dallas M, Lu Y, Zhao S, Harris M, Harris SE, Feng JQ, Bonewald LF. 2006. E11/gp38 selective expression in osteocytes: regulation by mechanical strain and role in dendrite elongation. Mol Cell Biol 26: 4539-4552.

Zhao M, Xiao G, Berry JE, Franceschi RT, Reddi A, Somerman MJ. 2002. Bone morphogenetic protein 2 induces dental follicle cells to differentiate toward a cementoblast/osteoblast phenotype. J Bone Miner Res 17: 1441-1451.

Zhao N, Nociti FH, Jr., Duan P, Prideaux M, Zhao H, Foster BL, Somerman MJ, Bonewald LF. 2016. Isolation and Functional Analysis of an Immortalized Murine Cementocyte Cell Line, IDG-CM6. J Bone Miner Res 31: 430-442.

Fig. 1 The floxed *Pdpn* allele in 126S6/C57BL6 mixed background showed a significantly reduced *Pdpn* Expression

A-C. Quantitative real time PCR for *Pdpn* expression. Data were collected from femur (A), kidney (B) and lung (C) of 3-month-old male mice. Sample sizes were 3, 7 and 1 for ($Pdpn^{+/+}$), heterozygous ($Pdpn^{fl/+}$) and homozygous ($Pdpn^{fl/fl}$) mice, respectively. The neomycin selection cassette was removed before setting up intercross of the heterozygous mice. Error bars are standard deviations. D. Presence of PDPN were detected using sections from kidney of 129S6 and C57BL6/J mixed background (129/B6). Bar = 20 μm E. Immunostaining for PDPN on vertebral sections (Cy3, red). The newly embedded osteocyte close to the bone surface were stained positive in the controls. The sections were counterstained with DAPI in blue. Differential interference contrast (DIC) of the same view is shown on the right. The Scale bar = 20 μm. N=2 for controls, n=2 for mutants.

Fig. 2 Surviving homozygous mice for the floxed *Pdpn* allele in 126S6/C57BL6 mixed background showed a reduced canalicular number with increased bone volume

A. X-ray radiograms of $Pdpn^{fl/+}$*;Ocn*-Cre (control, Cont) and $Pdpn^{fl/fl}$*;Ocn*-Cre (mutant, mut) mice at 3-month after birth. B-C. Acid-etched scanning electron micrograms of control (B) and mutant (C) tibia. Bar = 50 μm. D-E. Measurements of lacuno-canalicular network. F-G. microCT measurements of bone parameters in the trabecular compartment (F) and cortical compartment (G) of tibia. N=4 for controls, n=3 for mutants.

Fig. 3. *Pdpn* mutant mice have no overt abnormalities in bones.

A. Conversion of the *Pdpn*-floxed allele to a Cre-recombined allele. After confirmation of correct gene targeting event in embryonic stem cells and subsequent germ line transmission as detailed in Supplementary Fig 1, mice heterozygous for *Pdpn* floxed allele with a Pgk-neo cassette ($Pdpn^{fn/+}$) were bred with Flipper mice (Farley et al., 2000) to remove the neo cassette ($Pdpn^{fl/+}$). The $Pdpn^{fl/+}$ mice also were bred with *Sox2*-Cre mice (Hayashi et al., 2003) to delete exon 1 to generate a recombined null allele ($Pdpn^{+/-}$). B. Histologic observation of newborn stage lung. $Pdpn^{-/-}$ lungs characteristically show dense cellularity, narrow and tortuous air spaces, and thicker interalveolar septae compared to littermate control lungs. Paraffin sections (7 μm) stained with H&E. Bar = 50 μm. C. Histologic observations of calvaria, tibial growth plate, and metaphysis at E18.5. Paraffin sections (7 μm) were stained with H&E (upper), Picrosirius red (middle), or Von Kossa (lower). $Pdpn^{-/-}$ mice showed similar phenotypes of soft tissue, chondrocytes, mature collagen fiber, and calcified bone matrix with those found in littermate controls. Bar = 50 μm.

Fig. 4 *Pdpn* mutant mice show normal amelogenesis and odontogenesis.

Histologic observation and immunologic detection of podoplanin and amelogenin at E18.5. Coronal and sagittal paraffin sections (7 μm) were made for upper and lower incisor and molar and stained with H&E. Similar sections were used for immunofluorescent detections for Protein levels for podoplanin and amelogenin (arrowheads) for control ($Pdpn^{+/+}$) and homozygous null ($Pdpn^{-/-}$) mice. Bar = 50 μm.

Fig. 5 Surviving *Pdpn* mice in 126S6/C57BL6 mixed background showed liver abnormalities.

Livers were removed from 5-week-old *Pdpn*$^{+/-}$ and *Pdpn*$^{-/-}$ mice and production of PDPN (green), albumin (red), and CD90 (green) were detected using cryosections. Intensity of immunosignals for albumin was quantified (20 cells for each genotype). Positive cells for CD90 were counted using 2 sections per liver (200 cells for each genotype). Bar = 50 μm.

Fig. 6 Homozygous floxed *Pdpn* mice in Swiss background survived without PDPN protein.
Presence of PDPN were detected using sections from kidney, lung and bones prepared from Swiss background in wildtype but not null animals. Immunosignals were visualized by peroxidase reaction (kidney and lung) or a secondary antibody conjugated with Cy3 (bone, red). Bar = 20 μm.

Fig. 7 Homozygous null *Pdpn* mice in Swiss background did not show any overt bone phenotypes
A-C. X-ray radiograms of indicated bones from control (*Pdpn*$^{+/-}$) and homozygous mutant mice (*Pdpn*$^{-/-}$) at 6 months of age. D. Electron microscopy of acid-etched resin embedded bone shows the density and morphology of osteocyte lacunae and canaliculi in the cortical compartments of tibia. E. *Pdpn*$^{+/-}$ and *Pdpn*$^{-/-}$ mice were exercised on a treadmill for 3 weeks and morphology of osteocyte lacunae and canaliculi were revealed using electron microscopy of acid-etched resin embedded bone. The midshaft area of femoral cortical compartments were used as indicated as a yellow box on the right most panel.

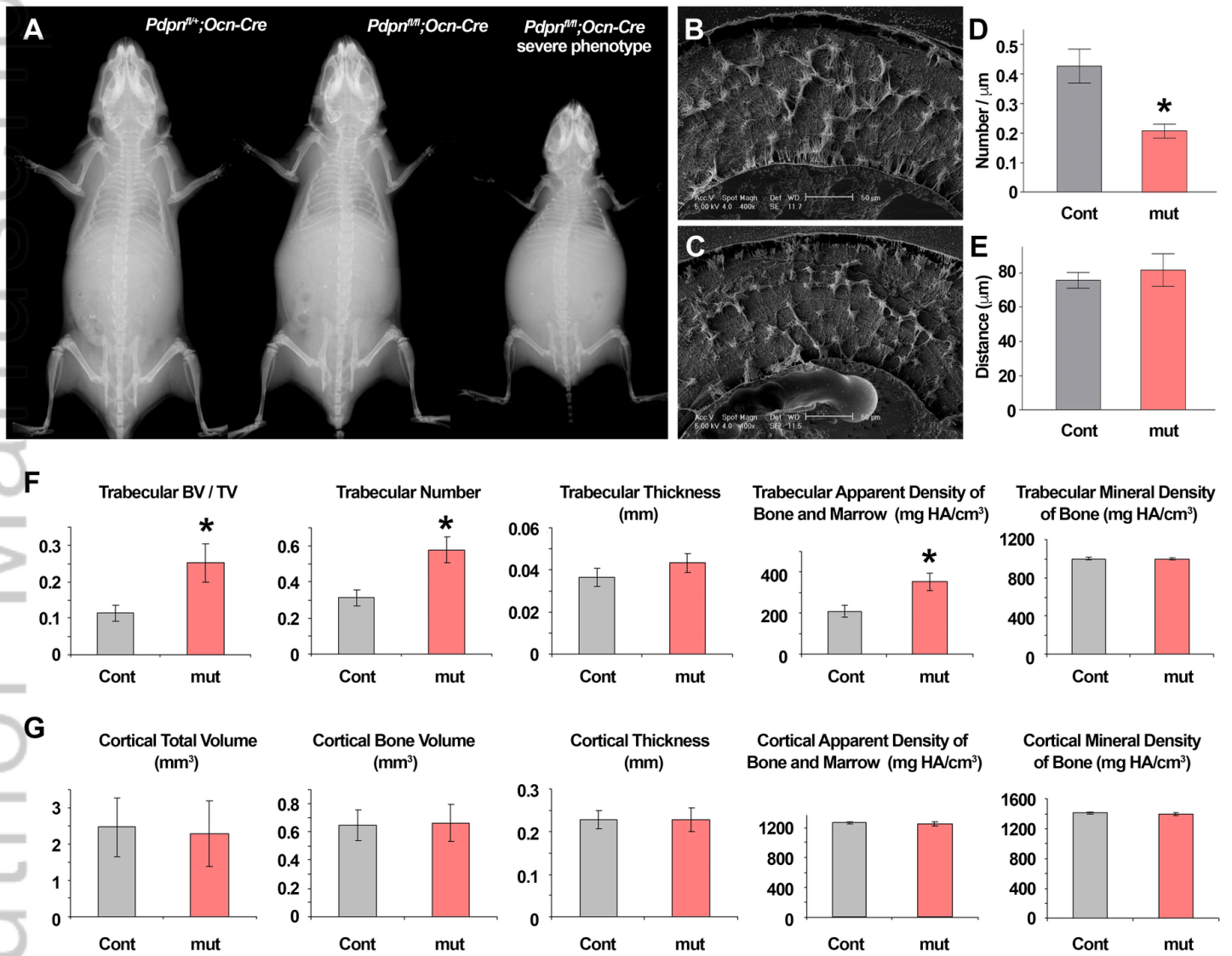**Supplementary Fig. 1 Targeting strategy to generate a *Pdpn* floxed allele**
To generate a floxed allele, a targeting vector to introduce one loxP into the 5'-UTR of the exon 1 and the other loxP into 1st intron was generated with a neomycin resistant cassette flanked with FRT sites. The linearized targeting vector was electroporated to embryonic stem (ES) cells (AB2.2 and UG347 lines) and correctly targeted clones were screened with Southern strategy as shown. Screened ES clones were subjected to blastocyst injection for germline transmission. Resulted F1 mice (*Pdpn*$^{fn/+}$) were bred with Flipper mice (Farley et al., 2000) to remove the neo cassette (*Pdpn*$^{fl/+}$). Resulted mice were further bred with *Sox2*-Cre transgenic mice (Hayashi et al., 2003) to remove the floxed region to inactivate gene function (*Pdpn*$^{+/-}$). Changes in gene structures were monitored by specific primers for each allele.

Primers; A (5'-CCCTAACAACCCCCTCCGC-3'),
B (5'-CCTCTTCAGGTCTATCCCCAGCC-3'),
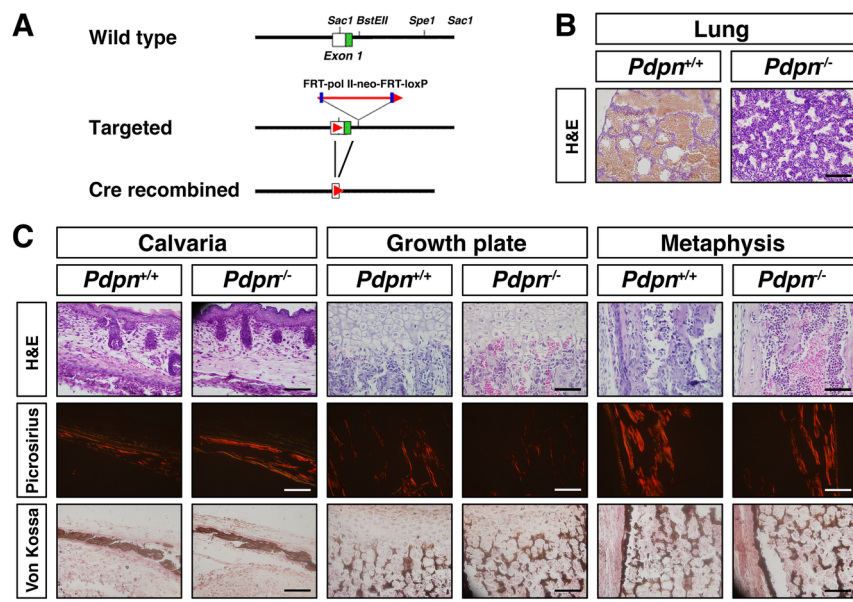C (5'-ACCGACACTCAGCACCATTTCC-3'),
D (5'-ATAAATGCCGACTGTGCCGAGAGG-3').
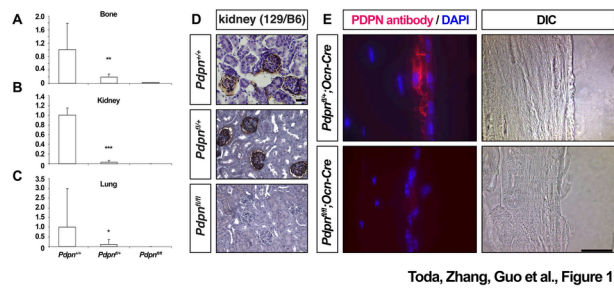
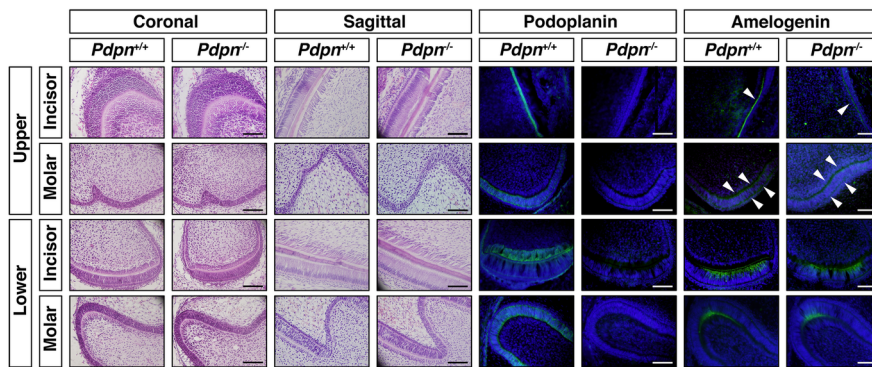Toda, Zhang, Guo et al., Figure 1

DVG_23450_Fig1.tif

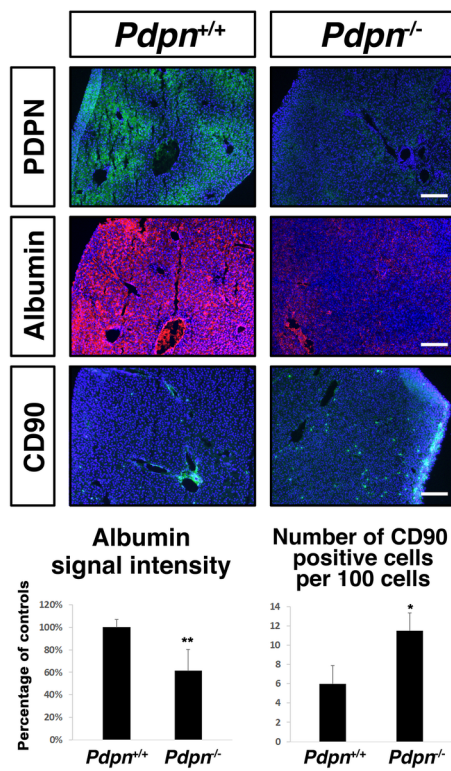Toda, Zhang, Guo et al., Figure 2

DVG_23450_Fig2.tif

A Wild type

Sac1 BstEII Spe1 Sac1

Exon 1

FRT-pol II-neo-FRT-loxP

Targeted

Cre recombined

B Lung

Pdpn⁺/⁺ *Pdpn*⁻/⁻

H&E

C

	Calvaria		Growth plate		Metaphysis	
	Pdpn⁺/⁺	*Pdpn*⁻/⁻	*Pdpn*⁺/⁺	*Pdpn*⁻/⁻	*Pdpn*⁺/⁺	*Pdpn*⁻/⁻
H&E						
Picrosirius						
Von Kossa						

Toda, Zhang, Guo et al., Figure 3

DVG_23450_Fig3.tif

Toda, Zhang, Guo et al., Figure 4

DVG_23450_Fig4s.tif

Toda, Zhang, Guo et al., Figure 5
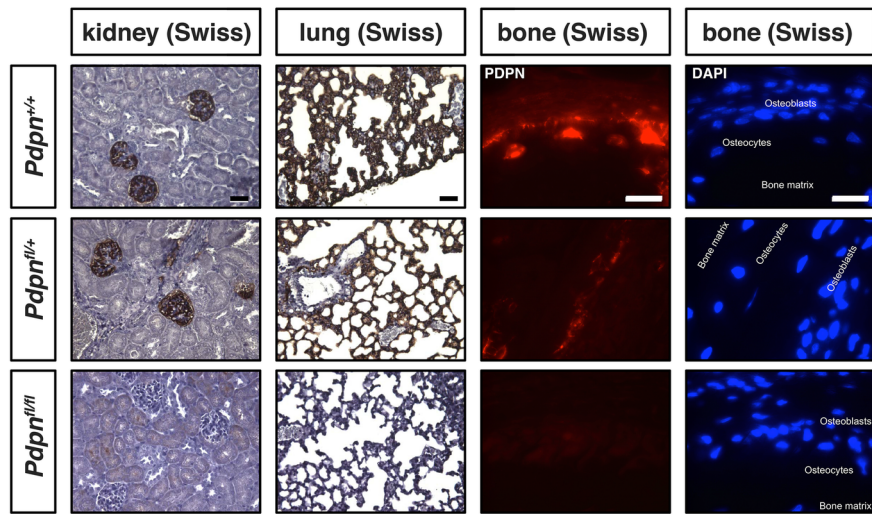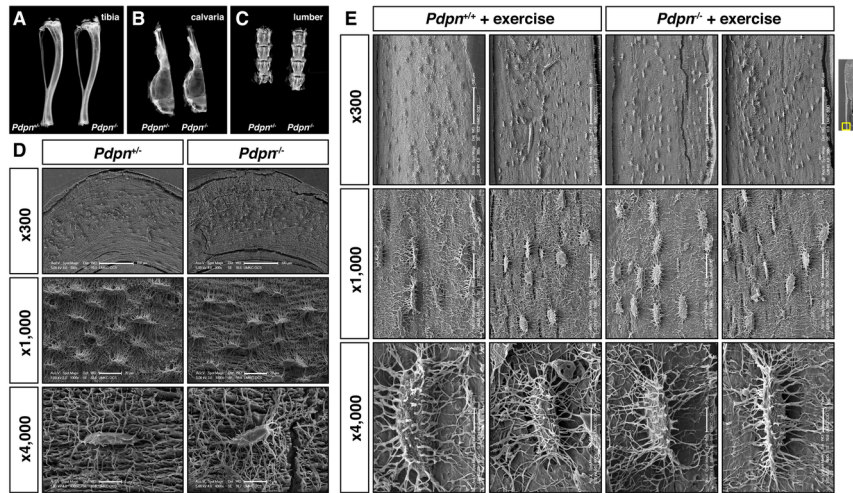
DVG_23450_Fig5-080321-3s.tif

	kidney (Swiss)	lung (Swiss)	bone (Swiss)	bone (Swiss)
Pdpn⁺/⁺			PDPN	DAPI
Pdpnfl/+				
Pdpnfl/fl				

Toda, Zhang, Guo et al., Figure 6

DVG_23450_Fig6s.tif

Toda, Zhang, Guo et al., Figure 7

DVG_23450_Fig7s.tif

Tables

Table 1. *Ratio of genotyping of offspring from the breeding between Pdpn floxed het mice*

background	stage	wild type (%) $Pdpn^{+/+}$	het (%) $Pdpn^{fl/+}$	homo (%) $Pdpn^{fl/fl}$	total	resorption site
129/B6$^\$$	3 weeks	29 (22.7)	58 (72.0)	6 (5.3)	93	n/a
129/B6	3 weeks	17 (31.2)	54 (62.3)	4 (6.5)	75	n/a
129/B6	E18.5	15 (21.4)	34 (48.6)	21 (30.0)	70	0
Swiss$^\&$	3 weeks	18 (37.0)	19 (47.8)	21 (15.2)	81	n/a
Swiss$^\#$	3 weeks	25 (36.8)	30 (44.1)	13 (19.1)	68	n/a
Swiss$^\#$	E18.5	13 (22.4)	31 (53.4)	14 (24.1)	58	n/a

$, floxed allele with the neo cassette; &, backcrossed one time; #, backcrossed twice.

Table 2. *Ratio of genotyping of offspring from the breeding of mice carrying the Cre-recombined Pdpn allele*

background	stage	wild type (%) $Pdpn^{+/+}$	het (%) $Pdpn^{+/-}$	homo (%) $Pdpn^{-/-}$	total
129/B6	E18.5	25 (22.7)	54 (49.1)	31 (28.2)	110
129/B6	3 weeks	13 (25.5)	34 (66.7)	4 (7.8)	51
Swiss$^\#$	3 weeks	4 (16.7)	15 (62.5)	5 (20.8)	24

#, backcrossed twice.